Figure S1

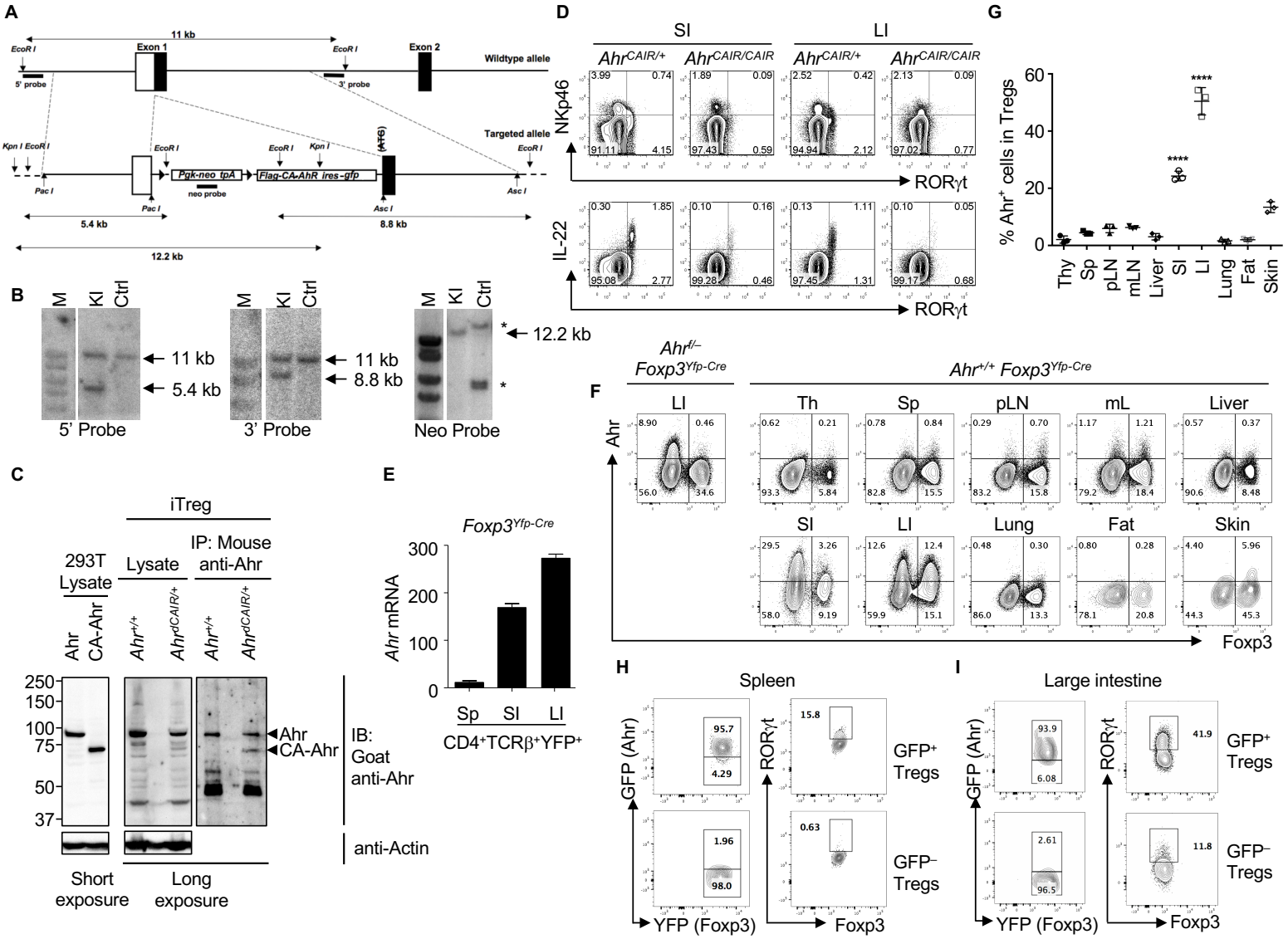

Figure S1 (Related to Figure 1). Generation of CA-Ahr conditional knock-in mice and determination of Ahr expression in different cell populations

(A) Targeting strategy for generation of *Ahr*^{CAIR} knock-in mice.

(B) Homologous recombination was confirmed by Southern blot using 5' probe with *Eco*R I digestion, 3' probe with *Eco*R I digestion, and neo probe with *Kpn* I digestion. * non-specific band.

(C) *Ahr*$^{dCAIR/+}$ mice were generated by crossing *Ahr*$^{CAIR/+}$ mice with *EIIa-cre* mice to delete the loxP-flanked STOP sequence in the germline, and subsequently removing the *EIIa-cre* transgene by breeding. CD4$^+$ T cells purified from the spleen of *Ahr*$^{+/+}$ or *Ahr*$^{dCAIR/+}$ mice were polarized under iTreg condition for 3.5 days. The cells were lysed and cell lysates were subjected to immunoprecipitation with mouse monoclonal anti-Ahr antibodies (RPT9, Novus). The immunoprecipitation sample were then subjected to immunoblotting using goat anti-Ahr antibody (N-19, Santa Cruz). As controls, HEK 293T cells were transfected with Flag-Ahr or Flag-CA-Ahr plasmid, respectively, and cell lysates were immunoblotted using goat anti-Ahr antibody (N-19). Anti-actin immunoblotting was performed as loading control.

(D) Flow cytometry analysis of RORγt, NKp46, and IL-22 expression gated on CD3$^-$ cells in the small (SI) and large intestinal (LI) lamina proprial leukocytes (LPLs) of *Ahr*$^{CAIR/+}$ or *Ahr*$^{CAIR/CAIR}$ mice.

(E) CD4$^+$TCRβ$^+$YFP$^+$ Tregs were sorted by FACS from the spleen (Sp), small (SI) and large intestine (LI) of *Foxp3*$^{Yfp\text{-}cre}$ mice. Relative expression of *Ahr* mRNA was analyzed by realtime RT-PCR.

(F) Flow cytometry analysis of Ahr and Foxp3 expression gated on CD4$^+$TCRβ$^+$ cells from the indicated tissues of *Ahr*$^{f/-}$*Foxp3*$^{Yfp\text{-}Cre}$ and *Ahr*$^{+/+}$*Foxp3*$^{Yfp\text{-}Cre}$ mice. Data are representative of three independent experiments.

(G) Percentages of Ahr$^+$ Tregs in various tissues of *Ahr*$^{+/+}$*Foxp3*$^{Yfp\text{-}Cre}$ mice. Data are shown as mean ± SD (n = 3). Thy: thymus; Sp: spleen; pLN: peripheral lymph nodes; mLN: mesenteric lymph nodes; SI; small intestine; LI: large intestine. ****$p \leq 0.0001$; ANOVA followed by Bonferroni's test for small intestine or large intestine versus other tissues.

(H and I) GFP$^+$YFP$^+$ Tregs and GFP$^-$YFP$^+$ Tregs from *Ahr*$^{CAIR/+}$*Foxp3*$^{Yfp\text{-}Cre}$ mice were sorted from the spleen (H) and large intestine (I) respectively and analyzed for the expression of RORγt and Foxp3. Data are representative from three independent experiments.

Figure S2

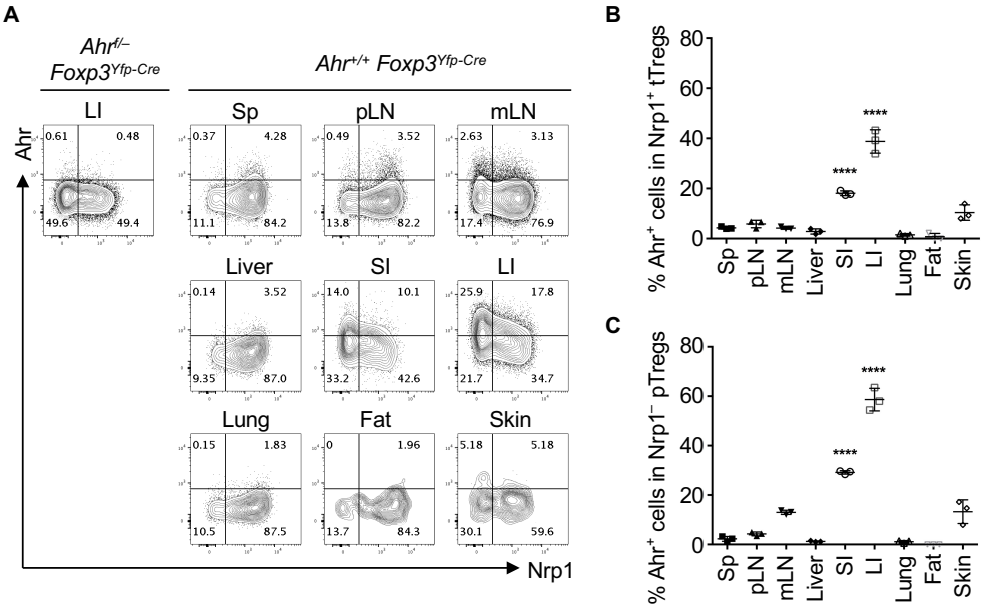

Figure S2 (Related to Figure 1).
(A) Flow cytometry analysis of Ahr and Nrp1 expression gated on CD4$^+$TCRβ$^+$Foxp3$^+$ Tregs from the indicated tissues of *Ahr$^{f/–}$Foxp3$^{Yfp\text{-}Cre}$* and *Ahr$^{+/+}$Foxp3$^{Yfp\text{-}Cre}$* mice.
(B, C) Percentages of Ahr$^+$ cells measured by intracellular staining in Nrp1$^+$ tTregs or Nrp1$^–$ pTregs in various tissues of *Ahr$^{+/+}$Foxp3$^{Yfp\text{-}Cre}$* mice. Data are shown as mean ± SD (n=3 mice per group). ****$p \leq 0.0001$; ANOVA followed by Bonferroni's test for small intestine or large intestine versus other tissues.
Sp: spleen; pLN: peripheral lymph nodes; mLN: mesenteric lymph nodes; SI; small intestine; LI: large intestine.

Figure S3

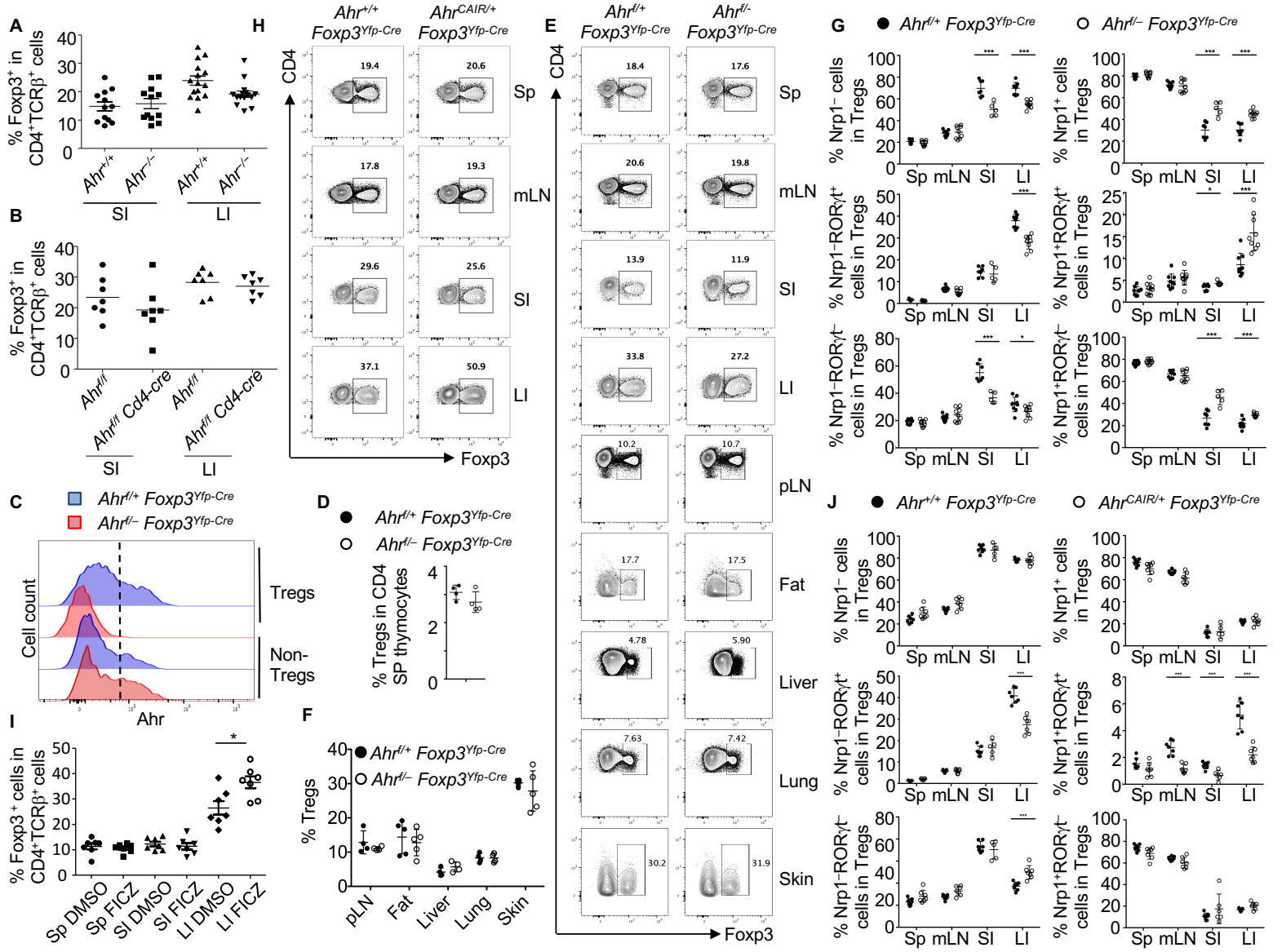

Figure S3 (Related to Figure 2).

(A-B) Percentages of Foxp3$^+$ Tregs among CD4$^+$TCRβ$^+$ cells in the small (SI) and large (LI) intestinal LPLs of *Ahr*$^{+/+}$ and *Ahr*$^{-/-}$ mice (A) or *Ahr*$^{f/f}$ and *Ahr*$^{f/f}$ *Cd4-cre* mice (B) (n = 7-15 per group)

(C) Flow cytometry analysis of Ahr expression gated on the CD4$^+$TCRβ$^+$Foxp3$^+$ Tregs or CD4$^+$TCRβ$^+$Foxp3$^-$ non-Tregs from the large intestine of *Ahr*$^{f/+}$*Foxp3*$^{Yfp\text{-}Cre}$ or *Ahr*$^{f/-}$*Foxp3*$^{Yfp\text{-}Cre}$ mice.

(D) Percentages of Foxp3$^+$ Tregs among CD4 single positive (SP) thymocytes in the *Ahr*$^{f/+}$*Foxp3*$^{Yfp\text{-}Cre}$ or *Ahr*$^{f/-}$*Foxp3*$^{Yfp\text{-}Cre}$ mice. Data are pooled from two independent experiments. Data shown as mean ± SD (n = 4 mice per group).

(E and F) Flow cytometry analysis (E) and percentage of Tregs gated on CD4$^+$TCRβ$^+$ cells from various tissues of the indicated littermate mice (F). Data are representative of three independent experiments. Data are shown as mean ± SD (n =5 mice per group).

(G and J) Percentages of Nrp1$^-$, Nrp1$^+$, Nrp1$^-$RORγt$^+$, Nrp1$^+$RORγt$^+$, Nrp1$^-$RORγt$^-$, or Nrp1$^+$RORγt$^-$ cells among CD4$^+$TCRβ$^+$Foxp3$^+$ Tregs in various tissues of the indicated mice. (I) 10-day-old wildtype mice were injected with FICZ or DMSO control for 7 days. Percentages of Foxp3$^+$ cells gated on CD4$^+$TCRβ$^+$ cells in various tissues were analyzed. Data are shown as mean ± SD (n =7 mice per group). *$p \leq 0.05$

Figure S4

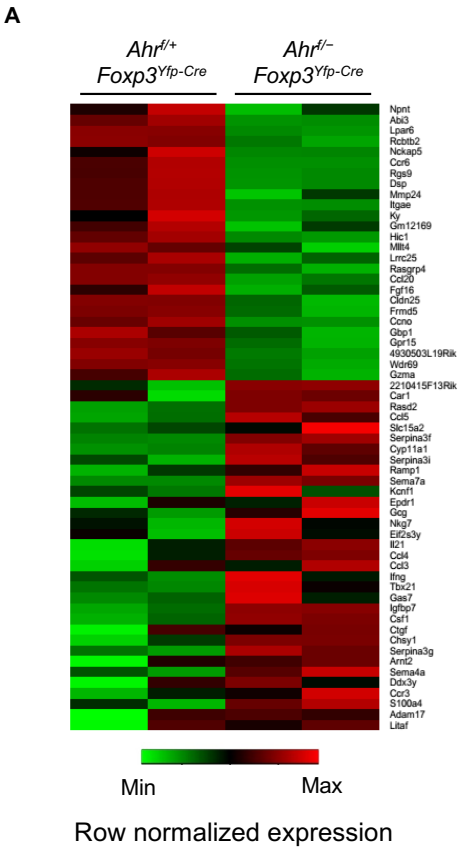

Figure S4 (Related to Figure 4).
(A) Heat map representation of genes with a statistical significant difference (q-value ≤ 0.05) between large intestinal Tregs from mice of the indicated genotypes (presented as k-means clustered and normalized gene expression).

Figure S5

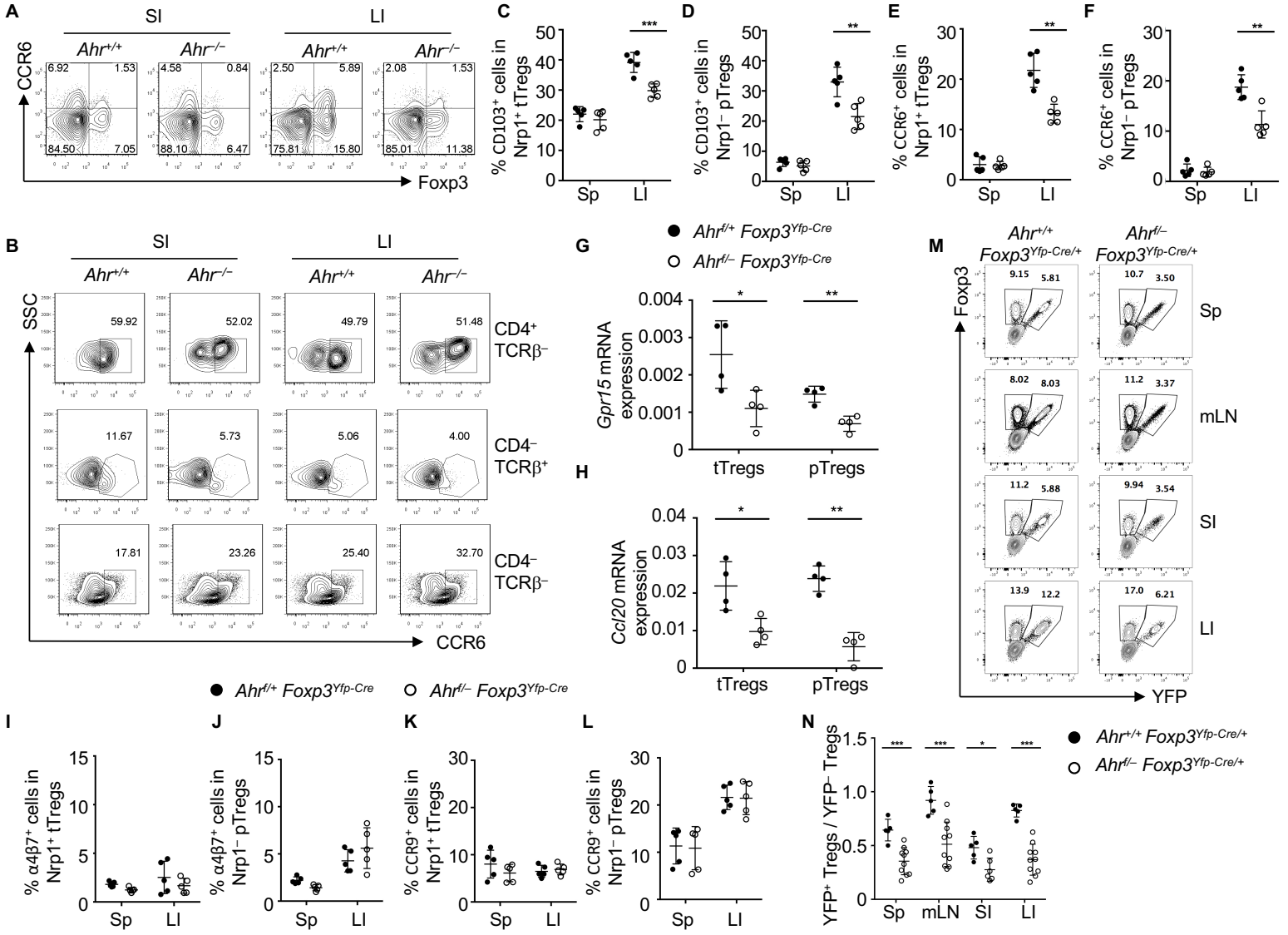

Figure S5 (Related to Figure 5).

(A) Flow cytometry analysis of CCR6 and Foxp3 expression gated on CD4$^+$TCRβ$^+$ cells in the SI and LI LPLs of *Ahr*$^{+/+}$ or *Ahr*$^{-/-}$ mice.

(B) Flow cytometry analysis of CCR6 expression gated on indicated populations in the SI and LI LPLs of *Ahr*$^{+/+}$ or *Ahr*$^{-/-}$ mice.

(C-F) Percentages of CD103$^+$ cells (C, D) and CCR6$^+$ cells (E, F) in splenic and large intestinal tTregs or pTregs of *Ahr*$^{f/+}$*Foxp3*$^{Yfp\text{-}Cre}$ or *Ahr*$^{f/-}$*Foxp3*$^{Yfp\text{-}Cre}$ mice. Data are compiled from three independent experiments and are shown as mean ± SD (n = 5 mice per group).

(G, H) CD4$^+$YFP$^+$Nrp1$^+$ tTregs or CD4$^+$YFP$^+$Nrp1$^-$ pTregs were sorted from the large intestine of *Ahr*$^{f/+}$*Foxp3*$^{Yfp\text{-}Cre}$ (Ctrl) or littermate *Ahr*$^{f/-}$*Foxp3*$^{Yfp\text{-}Cre}$ mice by flow cytometry. mRNA expression of *Gpr15* and *Ccl20* was analyzed by realtime RT-PCR. Dots are representative of biological repeats. Data are shown as mean ± SD (n = 4 mice per group).

(I-L) Percentages of α4β7$^+$ cells (I, J) and CCR9$^+$ cells (K, L) in splenic and large intestinal tTregs or pTregs of *Ahr*$^{f/+}$*Foxp3*$^{Yfp\text{-}Cre}$ or *Ahr*$^{f/-}$*Foxp3*$^{Yfp\text{-}Cre}$ mice. Data are compiled from three independent experiments and shown as mean ± SD (n = 5 mice per group).

(M) Flow cytometry analysis of Foxp3$^+$YFP$^-$ (Ahr wild-type) and Foxp3$^+$YFP$^+$ (Ahr KO) Tregs gated on CD4$^+$TCRβ$^+$ cells from various tissues of *Ahr*$^{+/+}$*Foxp3*$^{Yfp\text{-}Cre/+}$ or *Ahr*$^{f/-}$*Foxp3*$^{Yfp\text{-}Cre/+}$ female mice. Data are representative of three independent experiments.

(N) Ratio of YFP$^-$ Tregs / YFP$^+$ Tregs from various tissues of the indicated mice. Data were pooled from three independent experiments and are shown as mean ± SD (n = 5-10 mice per group). *$p \leq 0.05$, ***$p \leq 0.001$

Figure S6

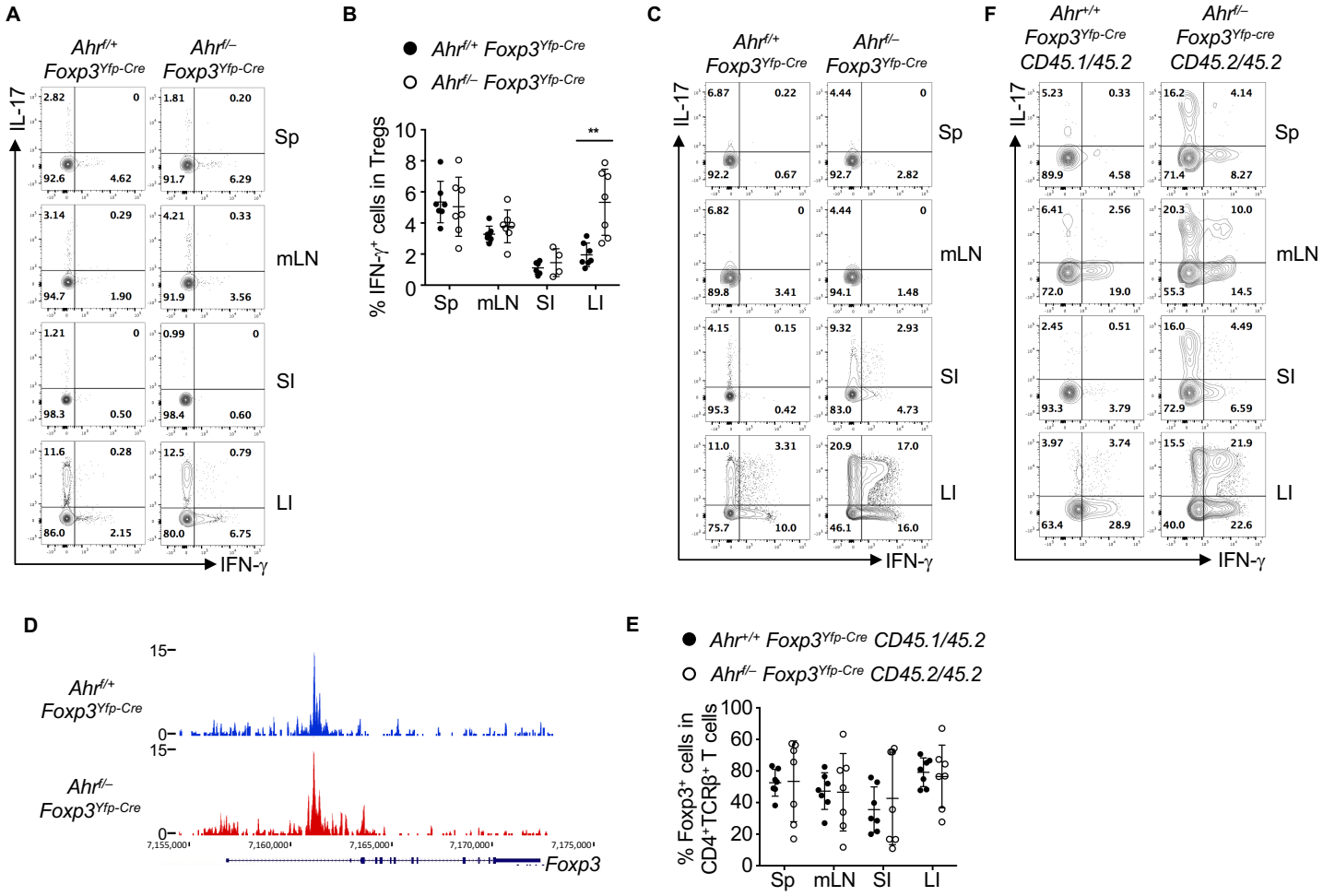

Figure S6 (Related to Figure 6).

(A) Flow cytometry analysis of IFN-γ and IL-17 measured by intracellular staining gated on CD4$^+$TCRβ$^+$Foxp3$^+$ Tregs from various tissues of *Ahr$^{f/+}$Foxp3$^{Yfp\text{-}Cre}$* and *Ahr$^{f/-}$Foxp3$^{Yfp\text{-}Cre}$* mice. Data are representative of two independent experiments.

(B) Percentages of IFN-γ$^+$ cells among Tregs in various tissues of the indicated mice. Data were compiled from two independent experiments and are shown as mean ± SD (n = 7 mice per group). $^{**}p \leq 0.01$

(C) CD4$^+$YFP$^+$(Foxp3$^+$) Tregs were purified from the spleen of *Ahr$^{f/+}$Foxp3$^{Yfp\text{-}Cre}$* or littermate *Ahr$^{f/-}$Foxp3$^{Yfp\text{-}Cre}$* mice. Around 2×10^5 cells from each group were transferred to *Rag1$^{-/-}$* mice. 3 weeks after transfer, mice were sacrificed for analysis. Expression of IFN-γ and IL-17 by Tregs was analyzed by intracellular staining followed by flow cytometry. Data are representative of two independent experiments.

(D) ATAC-seq signal profiles at the *Foxp3* locus in Tregs sorted from large intestinal LPLs of *Ahr$^{f/+}$Foxp3$^{Yfp\text{-}Cre}$* or littermate *Ahr$^{f/-}$Foxp3$^{Yfp\text{-}Cre}$* mice. Data are representative of two independent experiments.

(E-F) CD4$^+$YFP$^+$(Foxp3$^+$) Tregs were purified from the spleen of *Ahr$^{+/+}$Foxp3$^{Yfp\text{-}Cre}$ CD45.1/45.2* or *Ahr$^{f/-}$Foxp3$^{Yfp\text{-}Cre}$ CD45.2/45.2* mice and mix in 1:1 ratio. Around 4×10^5 mixed cells were transferred to *Rag1$^{-/-}$* mice. 3 weeks after transfer, mice were sacrificed for analysis. Percentages of Foxp3$^+$ Tregs among CD4$^+$TCRβ$^+$ cells derived from each congenically marked donor cells (E) and expression of IFN-γ and IL-17 by CD4$^+$TCRβ$^+$Foxp3$^+$ Tregs (F) are shown. Data are representative of two independent experiments and are shown as mean ± SD (n = 6 mice per group).

Figure S7

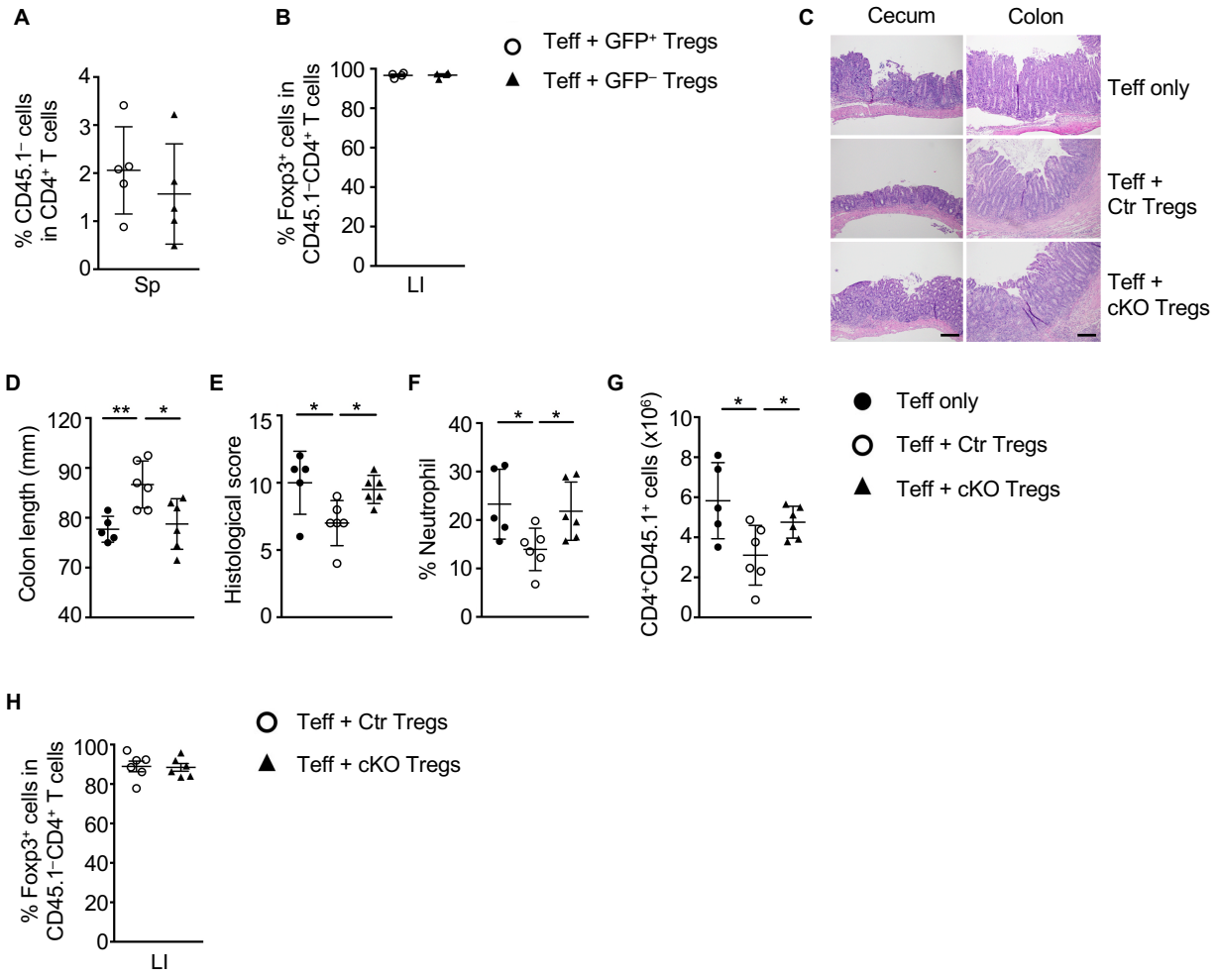

Figure S7 (Related to Figure 7).
(A and B) *Rag1*$^{-/-}$ mice were adoptively transferred with Teff with GFP^{+} or GFP^{-} Tregs as Figures 7C-I. Two weeks after transfer, the recipient mice were scarified and analyzed for the percentages of GFP^{+} or GFP^{-} CD45.1^{-} cells (i.e., donor Tregs) among CD4^{+} T cells in the spleen (A) and the percentages of Foxp3^{+} cells in donor Tregs in the large intestine (B). Data are representative of two independent experiments and are shown as mean ± SD (n= 4 mice per group).
(C-G) *Rag1*$^{-/-}$ mice were scarified 2 weeks after adoptive transfer of Teff without or with Tregs isolated from *Ahr*$^{fl/+}$*Foxp3*$^{Yfp\text{-}Cre}$ (Ctr) and *Ahr*$^{fl/-}$*Foxp3*$^{Yfp\text{-}Cre}$ (cKO) mice. Hematoxylin/eosin staining of cecum or colon, scale bar, 500 μm, (C), colon length (D), histology score (E), frequency of large intestinal infiltrating Gr-1^{+}CD11b^{+} neutrophils among CD45.2^{+} cells (F), absolute cell number of CD4^{+}CD45.1^{+} Teff cells in large intestinal LPLs (G), and the percentages of Foxp3^{+} cell in the Ctr or cKO donor cells (H). Data are representative of two independent experiments and are shown as mean ± SD (n= 5 to 6 mice per group).

Table S1 (Related to Figure 4, Figure 6, Figure S5 and Figure S6) Primers for Realtime RT-PCR and methylation assay:

Beta-actin FW	CTTCTTTGCAGCTCCTTCGTT
Beta-actin RV	AGGAGTCCTTCTGACCCATTC
Ahr FW	GGCTTTCAGCAGTCTGATGTC
Ahr RV	CATGAAAGAAGCGTTCTCTGG
Ahr Endogenous FW	CCACATCCGCATGATTAAGAC (Note: does not detect CA-Ahr cDNA)
Ahr Endogenous RV	TTCTGTAAATGCTCTCGTC (Note: does not detect CA-Ahr cDNA)
Itgae FW	TTCCCAGCAGATCCGAGCCTCC
Itgae RV	TGGGCAGTGCATCGGGGGTA
Cyp1a1 FW	GACATTTGAGAAGGGCCACAT
Cyp1a1 RV	TCCTGGATCTTTCTCTGTACCC
Gpr15 FW	TGGACCGTTACCTGGCTATC
Gpr15 RV	GCTCCCTGGACAGAAGAGTG
Ifng FW	AAATCCTGCAGAGCCAGATTA
Ifng RV	GTGGGTTGTTGACCTCAAACT
Tbx21 FW	AAGTTCAACCAGCACCAGACA
Tbx21 RV	GGTGGACATATAAGCGGTTCC
CCL5 FW	TCCAATCTTGCAGTCGTGTT
CCL5 RV	AGCAAGCAATGACAGGGAAG
CCL20 FW	CGTCTGCTCTTCCTTGCTTT
CCL20 RV	CGAGAGGCAACAGTCGTAGTT
Foxp3 TSDR FW	GGATTTGAATTGGATATGGTTTGTTTAG
Foxp3 TSDR RV	CAACCTTAAACCCCTCTAACATCCAAA

Supplemental Experimental Procedures

Generation of *Ahr*^{CAIR} Knock-in Mice

Flag-CA-Ahr (Ahr cDNA with deletion from aa 278 to aa 423) (Qiu et al., 2012) flanked by *Mlu* I and *Xho* I restriction enzyme sites was cloned into pIRES2-eGFP (Clontech) with engineered *Mlu* I and *Sal* I sites. The plasmid was then digested with *Nhe* I and *Not* I to obtain Flag-CA-Ahr-IRES-eGFP fragment that was subsequently cloned into pBigT (Srinivas et al., 2001). A 5′ homology arm of a 2.9-kb genomic fragment containing 5' UTR of exon 1 of *Ahr* gene and upstream DNA sequence was PCR amplified using C57BL/6 genomic DNA as template. A 3′ homology arm containing a 5.2-kb genomic fragment including coding region of exon 1 of *Ahr* gene without ATG and downstream DNA sequence was PCR amplified using C57BL/6 genomic DNA. The 5′ and 3′ homology arms were cloned in pBigT vector containing Flag-CA-Ahr-IRES-eGFP fragment at *Pac* I and *Asc* I sites, respectively. The sequence of the targeting construct was confirmed by DNA sequencing. The targeting construct was linearized by *Sal* I restriction enzyme and purified before electroporating into C57BL/6 ES cell line (PRX-B6) by Northwestern University Transgenic and Targeted Mutagenesis Laboratory, and neomycin resistant ES clones were screened for homologous recombination by Southern blot analysis using 5' and 3' probes with *Eco*R I restriction enzyme digestion or using Neo probe with *Kpn* I restriction enzyme digestion for homologous recombination. The verified clone was used for albino B6 blastocyst injection to generate male chimeric mice that were subsequently bred to albino B6 mice to test germline transmission. The targeted knock-in mice were designated *Ahr* $^{stop\text{-}Flag\ CA\text{-}Ahr\text{-}IRES\text{-}GFP}$, or *Ahr*^{CAIR} mice. When *Ahr*^{CAIR} mice are crossed with Cre-expressing transgenic mice, the Cre-mediated excision of the floxed termination sequence

(STOP: Pgk-neo-tpA) will lead to Flag-CA-Ahr-IRES-GFP expression in a cell type-specific manner.

iTreg in vitro differentiation

$CD4^+$ T cells were purified using mouse $CD4^+$ T cell isolation kit (Stemcell). 24-well plates were coated with 40 μg/ml anti-hamster antibody (MP Biomedical) at 37 ℃ for 4 hours. $CD4^+$ T cells were cultured in T cell media containing IMDM (Sigma-Aldrich) supplemented with soluble 0.25 μg/ml anti-mouse CD3 (145-2C11), 1 μg/ml anti-mouse CD28 (37.51), 2 μg/ml anti-mouse IL-4 (11B11), 2 μg/ml anti-mouse IFN-γ (XMG1.2) and 5 ng/ml TGF-β for 3.5 days.

RNA-seq and ATAC-seq data analysis

For RNA-seq data processing, barcoded samples were pooled and sequenced over 2 lanes on an Illumina HiSeq 2500 instrument to produce 50 bp single-end reads. De-multiplexed raw data files from the sequencing core were concatenated and uploaded to the Galaxy website for analysis (Blankenberg et al., 2010; Giardine et al., 2005; Goecks et al., 2010). Quality control data was generated with the NGS Toolbox quality control tools (Patel and Jain, 2012). Low-quality 3' bases were trimmed from each of the reads using the NGS Toolbox FASTQ trimmer tool (Patel and Jain, 2012). The trimmed reads were mapped (with TopHat2 fast splice junction mapper for RNA-Seq) to the January 2012 annotation of the *Mus musculus* genome (National Center for Biotechnology Information, mm9 assembly) and filtered for uniquely mapped reads (Kim et al., 2013). Genome visualization tracks (bedgraph files) were uploaded to UCSC Genome Browser for visual comparison of expression levels (Meyer et al., 2013; Patel and Jain, 2012). Quantitated relative mRNA expression levels (RPKM) were calculated based on exon regions using the SeqMonk software (Babraham Bioinformatics) and the mm9

reference genome annotations (Kent et al., 2002; Mortazavi et al., 2008). Significantly changed genes were found by the Intensity Difference method as outlined and recommended by SeqMonk documentation, and by DESeq analysis. Genes found to be significantly changed, after adjusting for multiple test comparisons, in both Seqmonk and DESeq (q-value $\leq$ 0.05, and filtered on max RPKM $\geq$ 1) were clustered (k-means) based on log2-transformed mean-centered RPKM values with the Cluster3 software (Anders and Huber, 2010; de Hoon et al., 2004; Eisen et al., 1998). The cluster analysis was visualized with gplots software (http://cran.r-project.org/web/packages/gplots).

For ATAC-seq data processing, ATAC-seq reads were mapped to the mouse genome (mm9) with bowtie2 (Langmead and Salzberg, 2012). The mapped reads were filtered using samtools (Li et al., 2009), keeping only the uniquely aligned reads, and bedgraph files (scaled to 10 million reads) were made with bedtools (Quinlan and Hall, 2010).

Supplemental References

Anders, S., and Huber, W. (2010). Differential expression analysis for sequence count data. Genome biology *11*, R106.

Blankenberg, D., Von Kuster, G., Coraor, N., Ananda, G., Lazarus, R., Mangan, M., Nekrutenko, A., and Taylor, J. (2010). Galaxy: a web-based genome analysis tool for experimentalists. Curr Protoc Mol Biol *Chapter 19*, Unit 19 10 11-21.

de Hoon, M.J., Imoto, S., Nolan, J., and Miyano, S. (2004). Open source clustering software. Bioinformatics *20*, 1453-1454.

Eisen, M.B., Spellman, P.T., Brown, P.O., and Botstein, D. (1998). Cluster analysis and display of genome-wide expression patterns. Proceedings of the National Academy of Sciences of the United States of America *95*, 14863-14868.

Giardine, B., Riemer, C., Hardison, R.C., Burhans, R., Elnitski, L., Shah, P., Zhang, Y., Blankenberg, D., Albert, I., Taylor, J.*, et al.* (2005). Galaxy: a platform for interactive large-scale genome analysis. Genome Res *15*, 1451-1455.

Goecks, J., Nekrutenko, A., Taylor, J., and Galaxy, T. (2010). Galaxy: a comprehensive approach for supporting accessible, reproducible, and transparent computational research in the life sciences. Genome biology *11*, R86.

Kent, W.J., Sugnet, C.W., Furey, T.S., Roskin, K.M., Pringle, T.H., Zahler, A.M., and Haussler, D. (2002). The human genome browser at UCSC. Genome Res *12*, 996-1006.

Kim, D., Pertea, G., Trapnell, C., Pimentel, H., Kelley, R., and Salzberg, S.L. (2013). TopHat2: accurate alignment of transcriptomes in the presence of insertions, deletions and gene fusions. Genome biology *14*, R36.

Langmead, B., and Salzberg, S.L. (2012). Fast gapped-read alignment with Bowtie 2. Nature methods *9*, 357-359.

Li, H., Handsaker, B., Wysoker, A., Fennell, T., Ruan, J., Homer, N., Marth, G., Abecasis, G., Durbin, R., and Genome Project Data Processing, S. (2009). The Sequence Alignment/Map format and SAMtools. Bioinformatics *25*, 2078-2079.

Meyer, L.R., Zweig, A.S., Hinrichs, A.S., Karolchik, D., Kuhn, R.M., Wong, M., Sloan, C.A., Rosenbloom, K.R., Roe, G., Rhead, B.*, et al.* (2013). The UCSC Genome Browser database: extensions and updates 2013. Nucleic acids research *41*, D64-69.

Mortazavi, A., Williams, B.A., McCue, K., Schaeffer, L., and Wold, B. (2008). Mapping and quantifying mammalian transcriptomes by RNA-Seq. Nature methods *5*, 621-628.

Patel, R.K., and Jain, M. (2012). NGS QC Toolkit: a toolkit for quality control of next generation sequencing data. PloS one *7*, e30619.

Qiu, J., Heller, J.J., Guo, X., Chen, Z.M., Fish, K., Fu, Y.X., and Zhou, L. (2012). The aryl hydrocarbon receptor regulates gut immunity through modulation of innate lymphoid cells. Immunity *36*, 92-104.

Quinlan, A.R., and Hall, I.M. (2010). BEDTools: a flexible suite of utilities for comparing genomic features. Bioinformatics *26*, 841-842.

Srinivas, S., Watanabe, T., Lin, C.S., William, C.M., Tanabe, Y., Jessell, T.M., and Costantini, F. (2001). Cre reporter strains produced by targeted insertion of EYFP and ECFP into the ROSA26 locus. BMC Dev Biol *1*, 4.